COMPUTATIONAL ASPECTS OF MUCUS PROPULSION BY CILIATED EPITHELIUM

Robin Chatelin, Philippe Poncet, Mayya Tokman

μFLU10-107

COMPUTATIONAL ASPECTS OF MUCUS PROPULSION BY CILIATED EPITHELIUM

Robin Chatelin, Philippe Poncet[1]
Toulouse Institute of Mathematics, CNRS UMR 5219 , Team MIP,
Dept. GMM, INSA, 135 avenue de Rangueil, F-31077 Toulouse, France
robin.chatelin@gmail.com, philippe.poncet@insa-toulouse.fr

Mayya Tokman
School of Natural Science, University of California,Merced
5200 N. Lake Rd. Merced, CA 95343, USA
mtokman@ucmerced.edu

KEY WORDS

Epithelium ciliated cells, lung mucus, numerical analysis, scientific computing.

ABSTRACT

This work is focused on the investigation of the mechanical dysfunction and airway clearance efficiency (or lack thereof) of the respiratory system by a quantitative analysis of mucus motion. We perform three-dimensional numerical simulations of the mucus and the ciliated cells present at lung walls (epithelium). In this preliminary work we consider a simplified configuration where the fluid is assumed to be Newtonian, the air/mucus interface is flat, and density and viscosity are constant. We formulate equations describing the simplified configuration, which are also relevant in the general context, and solve this system numerically to obtain mucus motion over a full cilia cycle. The stability condition of the explicit time integrators for the set of equations is prohibitively restrictive on the size of the integration time step. In order to begin development of effective numerical strategies for this problem we construct a one-dimensional model equation that contains the numerical challenges of a more general system. We study performance of several implicit and exponential time integrators using the model equation and use the results of the comparison to outline promising strategies for building efficient time integrators for a more complex system.

1. INTRODUCTION

Inhaled particles are removed from the respiratory tract by the mechanism of mucociliary clearance. The main assumption of mucociliary transport is that cilia of respiratory tract beat in a coordinated manner within the periciliary fluid underneath a layer of viscoelastic mucus gel. Inhaled airborne contaminants such as dust, micro-organisms, allergens or cellular debris are trapped in the mucus gel lining the conducting airways and then propelled out to be swallowed or expectorated.

Purkinje and Valentin first discovered the ciliary movement in the mammalian respiratory and reproductive tracts in 1834. This discovery was substantiated a year later when Sharpey indicated that mucus propulsion in the nose and trachea was associated with ciliary beating. Following this publication much information was gathered on ciliary movement although little of this data related to the respiratory tract. A 1928 literature review by Gray [8] stimulated work which led to the proposal by Lucas and Douglas [13] that cilia were bathed in a water-like fluid (the periciliary fluid) and with their tips sticking out into the mucus layer floating on the surface.

[1] Corresponding author

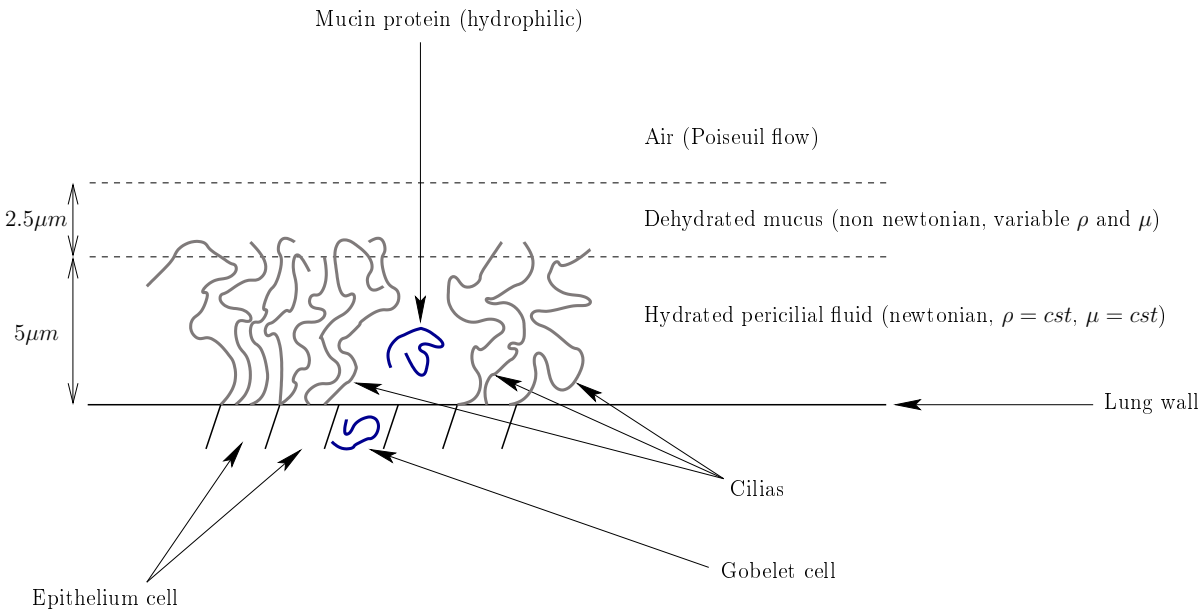

Figure 1: Typical configuration of mucus, ciliated and goblet cells near lung walls.

Although many advances in the knowledge of ciliary activity have followed this hypothesis, little attention was given to the respiratory tract. This was due in no small part to the abundance of cilia and flagella on more accessible surfaces. Fortunately, respiratory mucociliary clearance has been studied more extensively in recent years and most of what has been learned with other species appeared to apply.

Mucus is a visco-elastic fluid secreted by the respiratory epithelium that protects tracheo-bronchial tree mucosa from dehydration and traps inhaled particles (allergens, carcinogens, dust, micro-organisms, and inflammatory debris). It flows from either tracheo-bronchial tree or upper airways toward the pharynx, where it is swallowed (or expectorated).

A strong and effective mucus mobility is necessary to provide sufficient airway clearance and to ensure healthy behavior of the respiratory system. Stagnation or deficiency of mucus can cause pathogens to proliferate or to slip through pulmonary membrane. Respiratory diseases like cystic fibrosis (or mucoviscidosis), cilio-toxic affections (chronic bronchitis, virus and/or infections) or lung cancer can directly impact mucus motion by altering its viscosity, rheology, thickness, geometry, epithelium vibration features (cilia motion) or respiration cycle alterations. The present study aims at understanding the underlying mechanisms of these diseases.

In Section 2. physics and spatial scales of mucus layer and cilia are described and the parameters used for the numerical simulations of cilia motion and fluid dynamics are provided. Governing equations and numerical schemes are given in Section 3. and results are presented in section 4.. It is demonstrated that due to the microfluidics context development of an efficient numerical time integrator is key to performing computation over full cilium cycles even for a simplified configuration. In order to begin construction of an effective numerical algorithm for a more complex system in Section 5. we study performance of several implicit and exponential time integrators on a relevant one-dimensional model problem and use the results of the comparison to outline promising strategies for development of an efficient method for general system.

2. PROBLEM SETUP

The main objective of this work is to model and simulate motion of mucus in lungs. The tracheobronchial tree can be divided into three regions:

- the upper tree (generations 1 to 6)
- the small bronchi (generations 7 to 17)
- the acinus (generations 18 to 23)

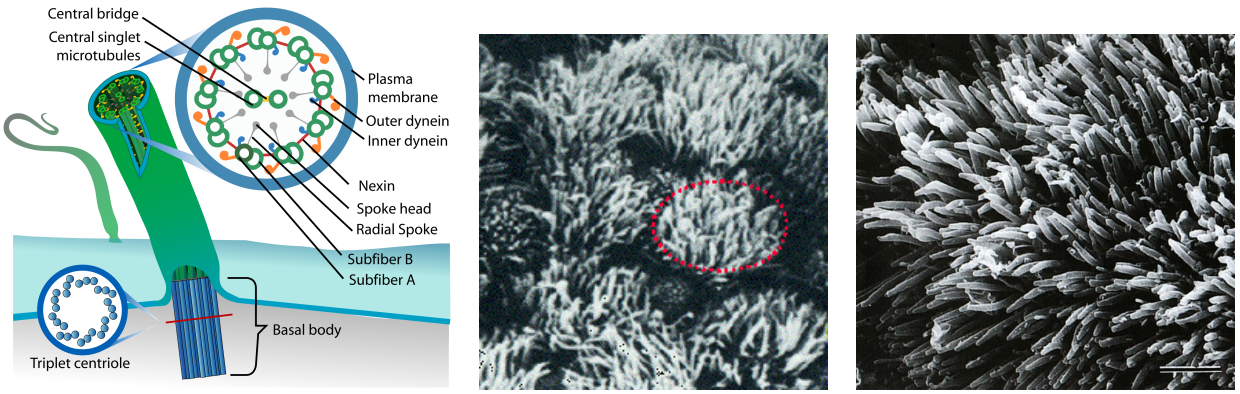

Figure 2: Polymer structure of a cilium (left picture, courtesy of M. R. Villareal), cilia cluster over an epithelium cell (middle picture), and cilia details in straight state (right picture, in vitro culture, from [22]). Bar is $2\mu m$.

where generations count the number of bronchiole divisions already occurred, the first generation being the trachea. Here we are only interested in modeling the flow in the generations 4 to 7, where the air has been warmed in the previous bronchi and the flow can be considered isothermal. Details on flows in other generations can be found in [14].

Lung walls are composed of epithelium cells and goblet cells (there are about four times more epithelium cells than goblet cells). The goblet cells release mucin proteins which hydrate the fluid whereas epithelium cells are composed of cilia which are oscillating to assure mucus transport. Thereby the domain geometry is complex and fast moving. Both solid deformations and fluid motion have to be taken into account. It will be assumed that the fluid is not deforming the solid, such approach is called one way fluid-structure interaction (in contrast with the one way / two ways interaction when structure is driving the fluid and fluid is deforming the structure).

In this part of the lung the flow has three phases and its general characteristics are presented on figure 1. The air flow is assumed to be a Poiseuille and two other fluid layers have to be distinguished. The first one is directly in contact with lung wall: this pericilial fluid is hydrated (the mucin protein produced by the goblet cells is hydrophilic and it carries water from other phase) so that it can be considered Newtonian with a low viscosity. The second mucus flow phase is located in the middle, between the Newtonian layer and the air. There mucus is dehydrated and is non-Newtonian. To model the respiration cycle, the Poiseuille air flow is assumed to be oscillating periodically at the frequency of the respiration cycle $(0.2 - 0.25Hz)$. The lung

walls are covered with both epithelium and goblet cells. This work is focused on studying the flow around one epithelium cell and the surrounding area, including cilia which is sometimes called motile. The motile cilia are usually present in large numbers on a cell's surface and beat in coordinated waves. Motile cilia can be found in the bronchial tree - figure 2 - where they sweep mucus and dirt out of the lungs. In female mammals, the beating of cilia in the Fallopian tubes moves the ovum from the ovary to the uterus. The role played by those cilia is not really well understood particularly as the driving mechanisms for the flow which is the subject of this research.

2.1 Epithelium and cilia desription

The beat cycle of respiratory cilia is composed of three phases: rest, recovery, and effective stroke. At rest, the cilium lies parallel to the bronchus wall pointing in the direction of mucus flow. The resting period separates effective stroke that is mostly planar with an arc of about 110 degrees and recovery stroke, during which cilia sweep backward remaining close to the epithelium and immersed in the periciliary fluid (without contact with the mucus layer). For the moment, to simplify the description, two cilia states are distinguished: a rest state and a straight state (figure 2).

A cilium is a tube which has a constant radius. Here we model a group of cilia by a succession of constant radius spheres separated by a constant distance. If the cilia is straight all the sphere centers are aligned (note

Symbol	Description	Value	Units
H_c	Cilium height	7	μm
R_c	Cilium radius	0.3	μm
N_c	Number of cilia per cell	4 or 16	-
N_s	Number of spheres per cilium	25	-
α	Angle between $z = 0$ plane and straight cilium	110	Degree
d_i	Distance between two cilia center	$4R_c$	μm
L_c	Length of the epithelium cell	$d_i\sqrt{N_c}$	μm
L_z	Edges length of the simulation box	12	μm
n_x	Number of space steps in direction x	32	-
n_y	Number of space steps in direction y	32	-
n_z	Number of space steps in direction z	32	-
T_{prop}	Propulsion time (from rest to straight)	17	ms
T_{ret}	Return time (from straight to rest)	34	ms
f_{tot}	Cilia oscillation frequency	20	Hz

Table 1: Values and description of the different parameters of the model.

that a straight cilium is not obviously vertical and it usually forms an angle with the lung wall at 110^o). Random process is used to provide a set of cilia at rest. A stiffening mechanism based on angle between three successive spheres along the cilium is provided in order to mimic the cilium beating cycle (see [5] for more details).

Two characteristic cilium positions have to be distinguished: straight (when all cilia are standing up) and resting (when cilia are fading like a wilted bunch of flowers). Cilium motion can be divided into two steps:

- Starting from straight configuration, cilia are moving for about $T_{ret} = 34ms$ until they reach the resting position.
- The second step is when cilia are recovering their straight state. It is quicker than the previous step and lasts about $T_{prop} = 17ms$. It is this last motion that supposedly propels the mucus.

Thus one full motion cycle last for approximately $T_{tot} = 51ms$ which means that cilia are oscillating at a frequency $f_{tot} = 19.6Hz$. All of the parameters cited in this section are summarized in table 1.

2.2 Mucus description and properties

From a macroscopic point of view mucus is a non-Newtonian thixotropic gel [12]. Its behaviour has to be distinguished from both solids and liquids by its response to shear stress :

- Under low shear mucus behaves like an elastic solid and regains shape over time;
- Under high shear mucus behaves like a viscous liquid and eventually deforms irreversibly.

The dynamic viscoelastic properties of mucus are constantly regulated to ensure an efficient clearance and to maintain sufficient adhesive strength to be retained on the epithelial surface despite external shearing forces (swallowing, gravity, surface tension, ...).

From a microscopic point of view mucus consists of mucins, DNA, lipids, ions, proteins, cells and cellular debris, water [11]... The biochemical regulation of these various constituents is complex and highly interdependent. A failure in any component can affect the physical properties of mucus and cause disease. Modifications in the rheological properties of mucus may greatly affect its ability to function as a selective barrier and the bronchi's first line of defense against infection. If mucus becomes too thick (in severe bronchitis for example the viscosity can be 100,000 times water's) patients experience great difficulty in mucus clearance. Such condition results in bacterial overgrowth and secondary infections can appear. On the other hand if viscosity is significantly lower the bronchi wall is underprotected and risk of infection increases.

There are two major mechanisms for clearing mucus from the tracheo-bronchial tree: by ciliary action (the primary mechanism) and by coughing when cilia fail or are overloaded. Methods for studying experimentally mucociliary clearance range from in vitro direct observation to in vivo tracer methods (using inhaled radio-labelled particles). Cough clearance can be studied in mechanical models with the use of appropriate tracers.

3. GOVERNING EQUATIONS

3.1 General governing equations

Fluid equations are derived from conservation laws; conservation of mass and conservation of momentum, i.e. the Newton's second law, give :

$$\partial_t \rho + \mathrm{div}\left(\rho u\right) = 0 \tag{1}$$

$$\partial_t \left(\rho u\right) + \mathrm{div}\left(\rho u \otimes u\right) - \mathrm{div}\sigma(u) = f \tag{2}$$

In these equations $\rho \in \mathbb{R}$ is the fluid density, $u \in \mathbb{R}^3$ the velocity, σ is the stress tensor and f contains the external forces applied to the fluid (in this model there is only gravity: $f = \rho g$). σ depends on fluid pressure $p \in \mathbb{R}$, the dynamic viscosity is $\mu \in \mathbb{R}$ and the deformation rate tensor $D(u)$ is given by

$$\sigma(u) = 2\mu\mathcal{F}(D(u)) - pId \tag{3}$$

where

$$D(u) = \frac{1}{2}\left(\nabla u + \nabla u^T\right). \tag{4}$$

In this section the model derived is generic and few assumption are made: fluid is considered to be non-Newtonian and incompressible, viscosity and density are non-constant. The incompressibility condition usually leads to the equation $\mathrm{div}u = 0$. This relation is valid for non constant density fluids [3], and for certain non isothermal fluids [4] and reactive flows [19].

Since $\mathrm{div}\left(\rho u \otimes u\right) = \rho u\left(\mathrm{div}u\right) + \rho\left(u \cdot \nabla\right)u + \left(u \cdot \nabla\rho\right)u$ the conservation of momentum equation can be rewritten as:

$$u\left(\partial_t\rho + u \cdot \nabla\rho + \rho\left(\mathrm{div}u\right)\right) + \rho\left(\partial_t u + \left(u \cdot \nabla\right)u\right) - \mathrm{div}\sigma(u) = f. \tag{5}$$

Using the mass conservation one finally obtains the Navier-Stokes equation in its standard form except for the diffusion term:

$$\rho\left(\partial_t u + \left(u \cdot \nabla\right)u\right) - \mathrm{div}\sigma(u) = f. \tag{6}$$

Another convection equation for μ has to be added since it can be variable with respect to both time and space :

$$\partial_t \mu + u \cdot \nabla\mu = 0 \tag{7}$$

This equation might be replaced by a law $\mu : \rho \longrightarrow \mu(\rho)$ in the future, which is equivalent to the convection equation when this law is linear.

3.2 Simplified model

In order to be able to determine the effects of cilia motion we consider a simplified model for the fluid. Indeed, we consider a Newtonian mucus, that is to say $\mathcal{F} \equiv Id$ or $\mathcal{F}(D) = D$, of constant density $\rho = 10^3\ kg{\cdot}m^{-3}$ and constant viscosity $\mu = 1$ (which is usually in the range $1 - 15Pa{\cdot}s$). Due to a very low value of the Reynolds number $Re \simeq 10^{-8}$ convection can be neglected [7] even when the boundaries are moving fast.

Moreover, we also assume that air-mucus interface is flat so the computational box only contains only mucus. Consequently surface tension does not have to be computed since the interface is not present in the equations.

Let Q the the computational box, and $B(t)$ the region inside the cilium. The fluid domain is then denoted $\Omega(t) = Q \setminus B(t)$, and the cilium/fluid interface is denoted $\Gamma(t) = \partial B(t)$. Given the assumptions above we obtain the Stokes equations with a complex moving geometry :

$$\frac{\partial u}{\partial t} - \frac{1}{\rho}\mathrm{div}\sigma(u) = g \text{ and } \mathrm{div}u = 0 \text{ in } \Omega(t), \text{ with } u = 0 \text{ on } \Gamma(t) \tag{8}$$

In order to handle the moving geometry, a penalization method (see [1] for instance) is applied to equation 8 : if $\bar{u}$ denotes the velocity inside the cilium, and $\chi_{B(t)}$ denotes the characteristic function of cilia (its value is 1 inside cilia and 0 otherwise), then the penalized equation is given by

$$\frac{\partial u}{\partial t} - \frac{1}{\rho}\mathrm{div}\sigma(u) = g - \frac{\chi_{B(t)}}{\varepsilon}(u - \bar{u}) \text{ and } \mathrm{div}u = 0 \text{ in } Q \tag{9}$$

where $\mathrm{div}\sigma(u) = \nu\Delta u + \nabla p$ and $\nu = \mu/\rho$ is the kinematic viscosity. In practice, ε is chosen as $\delta t/K$ with K in the range $1 - 10$.

A standard finite-difference schemes with pressure-velocity description inspired by the MAC algorithm has been implemented [5]. Backward Euler (implicit) method is employed for time integration: due to implicitness linear systems must be solved every time step. An explicit scheme would require a time step size of $\delta t \leq 10^{-13}$ due to stability restrictions. Since our goal is to run computations over a full cilium cycle of 0.05 seconds, implicit schemes allow to increase this time step up to $10^{-5} - 10^{-4}$ without any stability or accuracy problems. However, the matrix that has to be inverted each time iteration is badly conditioned. A GMRES algorithm [18] has been used to solve this linear system, which has allowed to perform a sufficient number of time iterations, as shown in section 4..
In order to improve the technique for solving such linear systems, a comparison between a few modern time integrators (adapted to such a complex shape of matrix) are provided in section 5.. Furthermore, future work will involve construction of characteristic methods for convection equation [17, 15] with variable density and/or viscosity fluids and improved particle schemes for diffusion computation [16].

4. RESULTS AND CHALLENGE

In the first numerical experiment we simulate four cilia. The results of the simulation are shown in figure 3. At the beginning of the simulation (first subplot) the cilia are straight and their motion is creating a velocity-norm-bubble around them. At the top there is a vortex like hollow in the velocity-bubble; as cilia tend to form a bunch when they are resting a depression is forming in the middle of the cell and it is creating this hollow in the velocity isosurface. Later in the simulation cilia are moving and the bubble is becoming larger and larger until it divides itself into four bubbles (one per cilium). Each velocity-bubble is then propagating and diffusing around its cilium. At the end of this subcycle velocity of the cilia is decreasing along with each velocity-bubble.

In figure 3 the second subcycle is presented with the same isosurface value. In the second part of this figure it can be observed that the beginning of the resting to straight position cycle is faster and each cilium also has its proper velocity-norm bubble. However, this time the velocity-bubbles are not dragged but propelled by the cilia until they form a bigger bubble in the middle of the cell. This bubble dissipates when cilia become close enough and stop moving. The simulation involving sixteen cilia, displayed in figure 5, shows the velocity field without isolated bubbles as cilia are closer to one another.

As the main interest of this work is to learn about the mucus displacement, especially at the air interface, figure 5 shows the x velocity components at the location $z = L_z/2$ at different times. When looking at the average velocity at the surface displayed in the right panel of figure 5 we notice that average displacement of the mucus surface over one cilia cycle is close to zero. The phenomenon is present even if there is no symmetry in the cilia motion : in the present case, the first part of the cycle (straight to rest, 2/3 of the cycle) is driven by random motion, while the second part (rest to straight, that is to say the stroke par, 1/3 of the cycle) is driven by stiffening motion.

Consequently, non-reversibility of the flows, that is to say good mucociliary clearance, is to be explained by another mechanism not yet investigated in our models. Possible explanation of non-reversibility requires the full

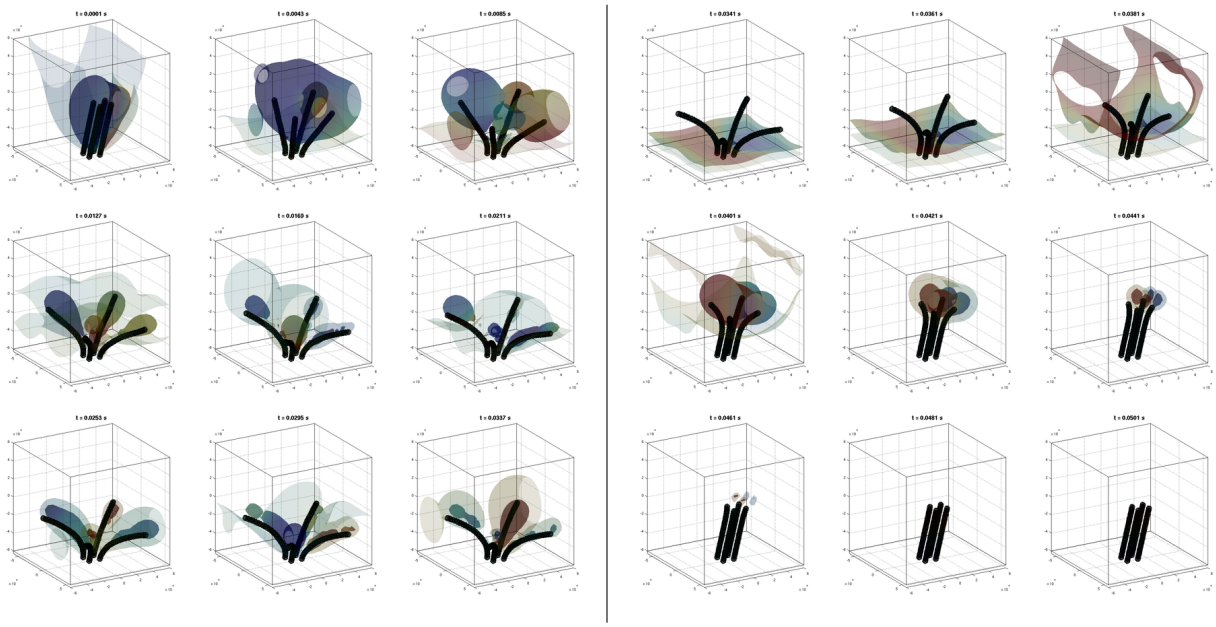

Figure 3: Velocity isosurfaces at level 5×10^{-9}, colored by the streamwise componant of velocity, at nine different times during the cycle from straight to rest (left pictures) and nine from rest to straight (right pictures). The simulation involves 32 mesh points in each direction, 4 cilia and 25 spheres per cilium. Computational domain is $12\mu m$ in each direction.

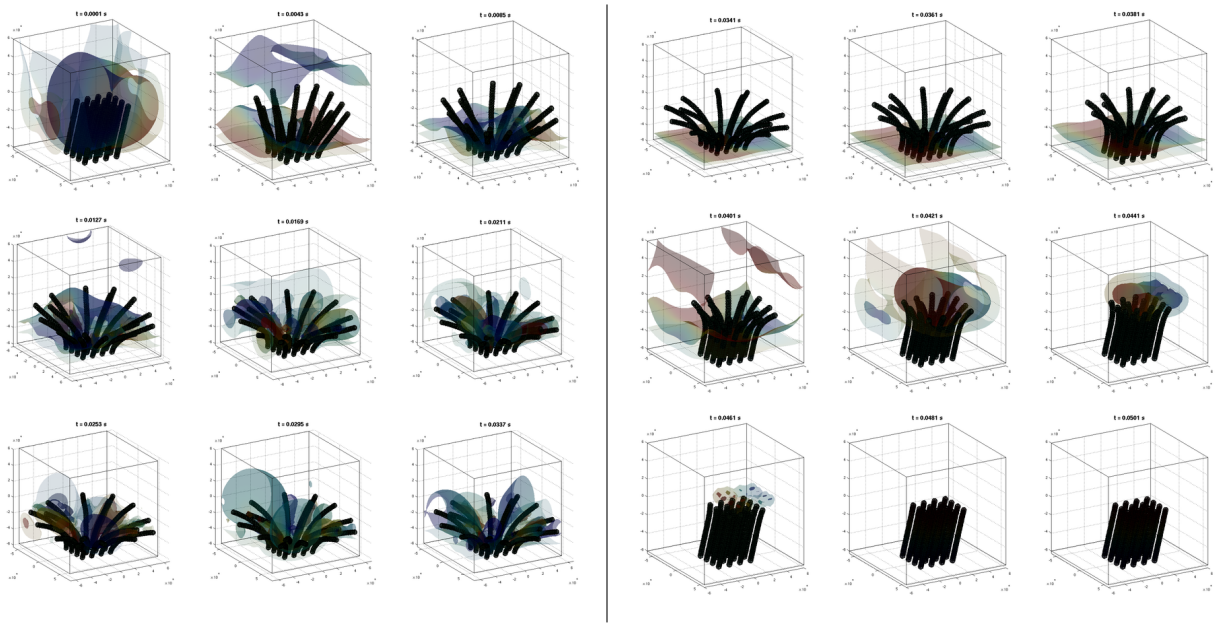

Figure 4: Same legend as figure 3 but for 16 cilia.

study of non-Newtonian and variable viscosity features of the mucus, the shape of the air-mucus interface, cell synchronization, and possibly other features of the system. Another possibility explaining the non-reversibility would be a poor efficiency of the beating sequence. Indeed, other beating cycles than the one presented here. Nevertheless, the one used presently is quite close to reality (2/3 at rest, 1/3 at stroke with final angle at 110^o), except for the random motion from stroke to rest.

In order to be able to simulate such significantly more complex systems over the time interval of interest we need to develop more efficient time integrators and improve computational performance by both allowing larger time steps (many orders of magnitude above standard CFL conditions) and reducing the computational cost of each time step. In the next section we study performance of several implicit and exponential integrators

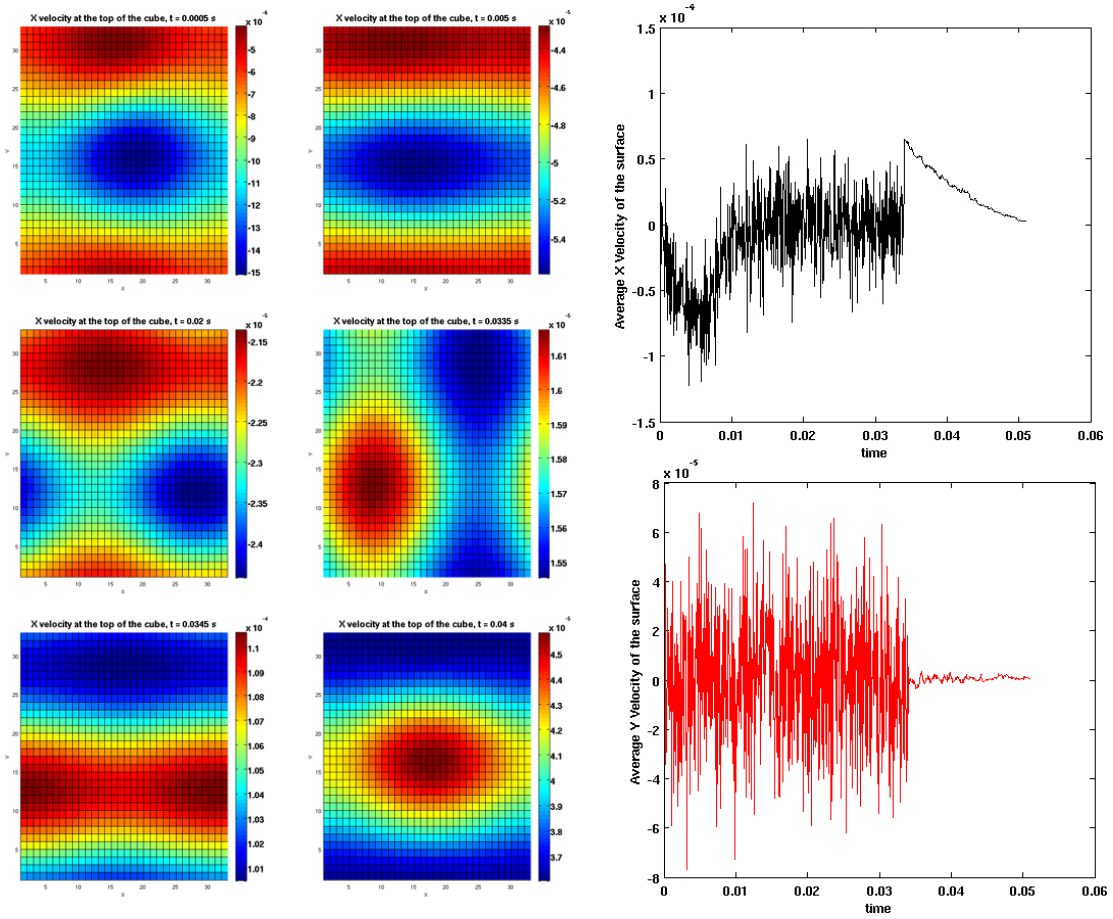

Figure 5: Profiles of the streamwise velocity component at the upper face of the cube (left picture), which can be as the mucus film top velocity, at six different times of the cilium cycle. Right pictures show the average velocity in streamwise (top right picture) and crosswise (bottom right picture) directions. Computational domain is $12\mu m$ in each direction.

on a one-dimensional equation that models numerical difficulties associated with a more complex system. These preliminary results point to promising strategies for constructing efficient time integrators for this system 3..

5. NUMERICAL STUDY OF TIME INTEGRATORS

In order to develop an effective time integration strategy for our system we study a one-dimensional model problem containing essential features of the equations. The velocity of the flow $u(x,t)$ is defined on an interval $x \in \Omega = [-L/2, L/2]$ and integrated for times $t \in [0,T]$, with $L = 2\,10^{-5}$.

The cilium is represented by a moving interval $B(t)$ whose boundaries are $X(t) \pm L/16$ with

$$X(t) = L\sin(2\pi t/T_p)/4$$

and a period of oscillation $T_p = 20$Hz. The model equation describing the velocity $u(x,t)$ for $x \in \Omega$, is given by equation 9, for which the one dimensional formulation is :

$$\frac{\partial u}{\partial t} = \alpha \frac{\partial^2 u}{\partial x^2} - \frac{1}{\varepsilon}\chi_{B(t)}(u - \bar{u}(t)), \tag{10}$$

with periodic boundary conditions, where

$$\chi_B(t) = \begin{cases} 1, & x \in B(t) \\ 0, & \text{otherwise} \end{cases}$$

and

$$\bar{u}(t) = \frac{\pi L}{2T_p}\cos(2\pi t/T_p)$$

is the prescribed velocity of the interval $B(t)$.

The parameter ε in the equation (10) is chosen based on the time-step as $\varepsilon = \delta t/8$ and $\alpha = 10^{-3}$ is the diffusion coefficient as described above in section 3.. The interval X represents a small portion of the mucus/cilia domain so periodic boundary conditions are imposed on $u(x,t)$.

To simplify our analysis the diffusion operator is discretized using second-order finite differences on N nodes. Note that the spectrum of the Jacobian of the equation (10) lies on the negative real line and can be calculated from the spectrum of the diffusion operator via shifting it to the left by $1/\varepsilon$. The presence of a wide spectrum of frequencies in the equation causes the problem to be stiff. Therefore special care must be taken in constructing a time integrator for the system.

Since ε is determined via establishing a time interval δt over which the model equation accurately represents the physical process, and the integration time interval T is typically very long compared to this time scale, it is desirable to use the same value δt for time stepping in the numerical integrator. However, explicit methods are bound by stability restrictions that require the time step size to be many orders of magnitude smaller than δt. This yields using explicit integrators computationally infeasible and forces us to resort to other numerical methods. Specifically, we study performance of implicit and exponential integrators whose stability properties are significantly better then those of explicit methods.

We need to investigate how the structure of the problem can be exploited to construct an efficient integrator. Therefore we begin our study by comparing the performance of several implicit and exponential methods. Anticipating a more complicated system we employ a splitting technique for all of these methods, i.e. the position and velocity of the interval $B(t)$ is assumed to be constant over each time step $t_n = t_0 + n\delta t$, the system is then integrated over the time interval $[t_n, t_{n+1}]$ and coordinates of $B(t)$ are updated for the next time step.

Implicit methods are usually algorithms of choice for stiff problems, we solve discretized in space system using Implicit Euler (IE), Crank-Nicolson (CN) and second-order backward-differentiation formula (BDF2) methods. If the linear system of ODEs we need to solve is written as

$$\begin{aligned} &\frac{dU}{dt} = F(U) = AU + b \\ &U(t_0) = U_0, \quad U, b \in \mathbf{R}^N, A \in \mathbf{R}^{N\times N} \end{aligned} \tag{11}$$

all of these implicit schemes can be represented by an equation

$$U_{n+1} = (I - \gamma\delta t A)^{-1}\delta t F(U_n) + W_n, \tag{12}$$

where parameter γ and vector W_n are defined for each of the methods.

A more recent development in numerical methods for stiff ODEs is construction of exponential integrators [9]. In case of general nonlinear system many exponential integrators can be constructed, but for the linear equation (11) all these methods are reduced to an exponential Euler method

$$U_{n+1} = U_n + \varphi_1(\delta t A)F(U_n), \tag{13}$$

where $\varphi_1(z) = (e^z - 1)z^{-1}$.

Since the Jacobian matrix of the more complex three-dimensional model is expected to be non-symmetric and stiff, the solution of the linear system resulting from implicitness or the evaluation of an exponential-type function of a Jacobian will constitute the primary computational cost of an implicit or an exponential time integrator. A usual method of choice to evaluate a product of an inverse or an exponential of a large matrix with a vector is a Krylov projection based algorithm. Thus we test implicit methods coupled with a GMRES

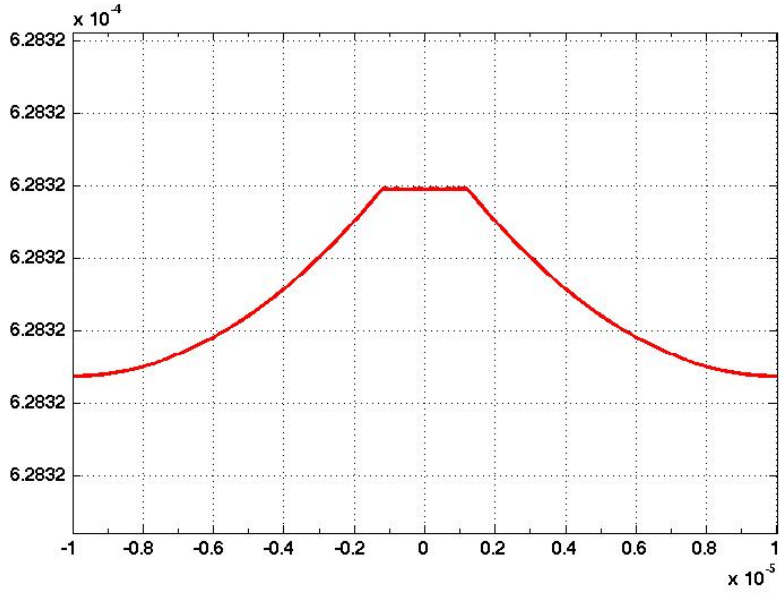

Figure 6: Solution $u(x,t)$ to the equation (10) at $t = 0.1$ with $\delta t = 10^{-4}$.

	Average performance data per time step				
$N = 300$	Implicit Euler-Krylov	BDF2-Krylov	Crank-Nicolson-Krylov	Exp-Pade	Exp-Krylov
Error	7.08E-07	6.43E-07	2.83E-06	1.90E-9	1.90E-9
CPU time	5.46E-01	5.45E-01	5.45E-01	6.65E-01	4.86E-01
Krylov iterations	264	264	264	n/a	267

Table 2: Comparative performance of implicit and exponential integrators for the 1D model problem (10).

algorithm for solving the linear systems and an exponential-Krylov integrator. Since our test problem is small we validate the accuracy of the solution by computing the inverse and the exponential using computationally intensive but reliable methods such as direct solvers for the linear systems and high-order Pade approximations for the exponential.

Figure (10) displays the solution $u(x,t)$ at $t = 0.1$ with $\delta t = 10^{-4}$ computed using exponential-Krylov methods. Since the velocity of the interval $B(t)$ is known and should match the velocity of the flow at the interface we use the difference between the flow velocity at the point closest to the endpoint of the oscillating interval $B(t)$ and its velocity as a measure of the error. The tolerance for the Krylov iteration is set artificially high at 10^{-13}, this is done across the methods to obtain fair comparisons. Table 5. lists the averages per time step of the infinity norm of the absolute error, the CPU time and, if applicable, the number of Krylov iterations per time step for all the methods.

The following conclusions can be drawn from the performance comparison. The presence of the corners in the solution at the interface between the flow and the oscillating interval $B(t)$ significantly influences all of the integration methods. Specifically, as is well known the Crank-Nicolson scheme contains oscillations when the solution is not smooth. Thus the error of the CN scheme is the largest among the methods. More importantly, the Krylov iteration is also affected by the lack of smoothness in the solution, i.e. the number of Krylov vectors needed to achieve the prescribed accuracy is very high for all of the methods (this remains true as the number of spatial grid points N is varied). In general, the convergence of the Krylov iteration to approximate a product of a matrix function with a vector $f(A)v$ depends on the structure of A, the function $f(z)$ and the vector v. For smooth solutions exponential functions, e.g. $f(z) = \varphi_1(z)$ require fewer Krylov iterations compared to the rational function $f(z) = 1/(1-z)$, that is to say $f(z) = (I-z)^{-1}$ when applied to matrix [21]. However, for this problem the lack of smoothness results in the structure of A and the vector v becoming the most important factors for the convergence of Krylov iteration. The presence of large amplitude high frequencies in the solution

requires a large portion of the spectrum of A to be resolved before an accurate solution can be computed. This realization directs us to seek non-Krylov based methods or to regularize the model to design an effective time integration scheme for the general model.

Another observation that can be made from Table 5. is the higher accuracy of the exponential integrators compared to the implicit methods. This is explained by the fact that exponential integrators approximate the solution directly while the implicit methods approximate the exact solution by a rational function. At the same time the CPU time required by either implicit or exponential methods is comparable (surely, the execution time depends on the implementation, but these preliminary results serve as a good guideline). Thus we conclude that constructing a non-Krylov based exponential integrator for the general system could be the most efficient way to solve the general system. Using contour integration to evaluate the exponential function $\varphi_1(z)$ [10, 2] could provide a more efficient algorithm. To summarize, our preliminary results helped to better understand the numerical difficulties associated with solving the system and revealed promising directions in constructing efficient time integrators for this problem. We plan to pursue these directions in the future.

6. CONCLUSIONS AND FUTURE WORK

We have built a set of model equations in order to be able to numerically study the interactions between ciliated cells and their surrounding mucus film in human lungs. The relevant spatial scales have been described with characteristic lengths ranging between $100nm$ for cilium diameter to $10\mu m$ for mucus film thickness.

We have focused our efforts on the geometric aspects in the present work and a simple model for the fluid has been considered : Newtonian nature has been assumed for mucus, the air-mucus interface is taken to be flat, and the density and viscosity are set to be constant in space. It has been shown in previous works that air-mucus coupling cannot be responsible for mucus transport under normal conditions. The preliminary results obtained with this simplified configuration indicate that there is no significant non-reversibility of mucus displacement in this case, so the main mechanism of mucus motion is still unclear.

We have also investigated challenges associated with solving the model equations numerically. We found explicit integrators to be too inefficient due to their poor stability properties and used implicit Euler method to carry out the calculations. In addition, we have studied performance of several implicit and exponential integrators on a model system and found that the exponential integrators can be more accurate then implicit methods. Our comparisons shed light on the numerical properties of the system and suggested that time integrators which couple exponential propagation with contour integration-based evaluation of exponential functions can potentially offer significant computational advantages in modeling mucus motility. We plan to pursue construction of such integrators in the future. We will use progress in increasing computational efficiency of the numerical methods to simulate more complex models of mucus motion and to conduct more detailed studies of the mechanisms of mucociliary clearance in lungs.

REFERENCES

[1] Angot, P., Bruneau, C.-H. & Fabrie, P. (1999). A penalization method to take into account obstacles in incompressible viscous flows. Numerische Mathematik 81(4):497-520.

[2] Caliari, M. & Ostermann, A. (2009). Implementation of exponential Rosenbrock-type integrators. Appl. Numer. Math. 59:568-581.

[3] Chassaing, P., Antonia, R. A., Anselmet, F., Joly, L. &Sarkar, S. (2002). Variable Density Fluid Turbulence. Kluwer Academic Publisher.

[4] Chenoweth, D. R. & Paolucci, S. (1985). Gas flow in vertical slots with large horizontal temperature differences. Physics of Fluids 28:2365.

[5] Chatelin, R. (2010). Contribution to three-dimensional computation of interaction between ciliated epithelium and mucus film in lungs. Master Thesis, University Paul Sabatier, Toulouse III, France.

[6] Cottet, G-H., & Poncet, P. (2003). Advances in Direct Numerical Simulations of three-dimensional wall-bounded flows by Particle in Cell methods. J. Comp. Phys. 193:136-158.
[7] Enault, S., Lombardi, D., Poncet, P., & Thiriet, M. (2010). Mucus dynamics subject to air and wall motion. ESAIM Proceedings 30:125-141
[8] Gray, J. (1928). Ciliary movement. Cambridge University Press.
[9] Hochbruck M., & Ostermann, A. (2010). Exponential integrators. Acta Numerica 19:209-286.
[10] Kassam, A. K., & Trefethen, L. N. (2005). Fourth-order time stepping for stiff PDEs. SIAM J. Sci. Comput. 26(4):1214-1233.
[11] King, M. (1998). Experimental models for studying mucociliary clearance. Eur. Respir. J. 11(1):222-228.
[12] Lai, S. K., Wang, Y. Y., Wirtz, D. & Hanes, J. (2009). Micro- and macrorheology of mucus. Advanced Drug Delivery Reviews 61(2):86100.
[13] Lucas, A. M. & Douglas, L. C. (1934). Principles underlying ciliary activity in the respiratory tract. ii. a comparison of nasal clearance in man, monkey and other mammals. Arch. Otolaryng. 20:518-541.
[14] Mauroy, B. (2004). Hydrodynamique dans le poumon, relations entre flux et géométries. PhD thesis, ENS Cachan.
[15] Poncet, P., Hildebrand, R., Cottet G-H., & Koumoutsakos, P. (2008). Spatially distributed control for optimal drag reduction of the flow past a circular cylinder. J. Fluid Mech. 599:111-120.
[16] Poncet, P. (2006). Finite difference stencils based on particle strength exchange schemes for improvement of vortex methods. J. Turbulence 7 (23):1-24.
[17] Poncet, P. (2004). Topological aspects of the three-dimensional wake behind rotary oscillating circular cylinder. J. Fluid Mech. 517:27-53.
[18] Saad, Y. & Schultz, M. H. (1986). GMRES: A generalized minimal residual algorithm for solving non-symmetric linear systems. SIAM J. Sci. Stat. Comput. 7(3):856-869.
[19] Sandoval, D. L. (1995). The dynamics of variable-density turbulence. PhD thesis, LA-13037-T, Los Alamos National Lab., NM (USA).
[20] Tokman, M. (2006). Efficient Integration of Large Stiff Systems of ODEs with Exponential Propagation Iterative (EPI) Methods. J. Comp. Phys. 213:748-776.
[21] Tokman, M., & Loffeld, J. (2010). Efficient design of exponential-krylov integrators for large scale computing. Proceedings of the 10th International Conference on Computational Science, Procedia Computer Science (in press).
[22] Yoshitsugu, M. , Hanamure, Y., Furuta, S., Deguchi, F., Ueno, K. & Rautiainen, M. (1994). Ciliary motility and surface morphology of cultured human respiratory epithelial cells during ciliogenesis. Biol. Cell. 82:211-216.